Article

Cell Stem Cell

In Vitro Expansion of Primary Human Hepatocytes with Efficient Liver Repopulation Capacity

Graphical Abstract

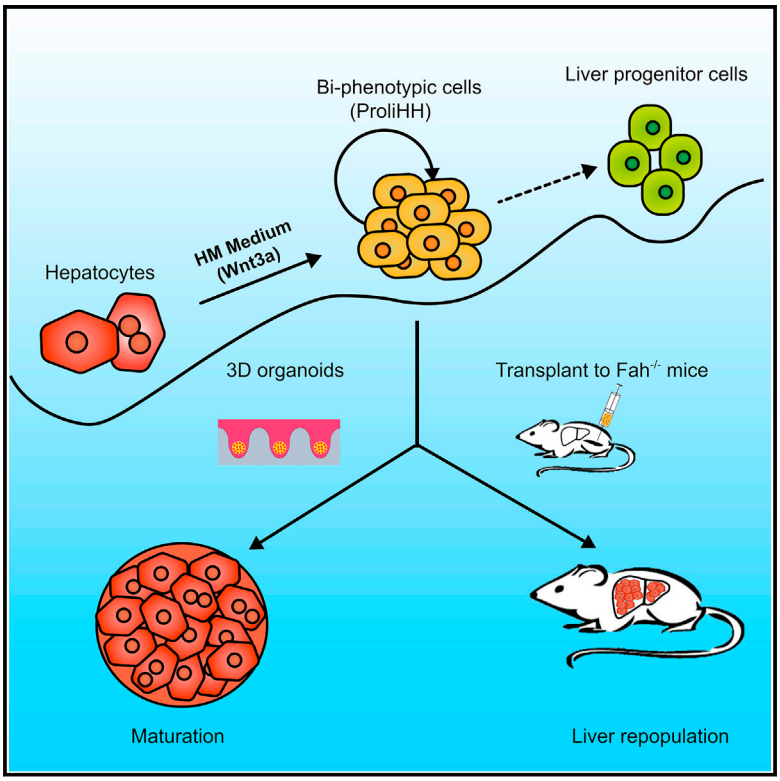

Authors

Kun Zhang, Ludi Zhang, Wenming Liu, ..., Dong Gao, Luying Peng, Lijian Hui

Correspondence

zhangludi@sibcb.ac.cn (L.Z.), luyingpeng@tongji.edu.cn (L.P.), ljhui@sibcb.ac.cn (L.H.)

In Brief

Hui et al. developed a defined medium to expand primary human hepatocytes to a large quantity. Proliferating human hepatocytes show both hepatocyte and progenitor features and could be reverted to mature phenotypes in an organoid culture and notably can repopulate mouse livers with high efficiency.

Highlights

- Human hepatocytes can be serially passaged and expanded 10,000-fold
- Proliferating HHs (ProliHHs) display hepatic features and express progenitor markers
- ProliHHs can mature following *in vitro* differentiation or transplantation
- ProliHHs repopulate injured livers with comparable efficiency to primary hepatocytes

Data Resources

GSE112866

Zhang et al., 2018, Cell Stem Cell *23*, 1–14
December 6, 2018
https://doi.org/10.1016/j.stem.2018.10.018

CellPress

Please cite this article in press as: Zhang et al., *In Vitro* Expansion of Primary Human Hepatocytes with Efficient Liver Repopulation Capacity, Cell Stem Cell (2018), https://doi.org/10.1016/j.stem.2018.10.018

Cell Stem Cell
Article

In Vitro Expansion of Primary Human Hepatocytes with Efficient Liver Repopulation Capacity

Kun Zhang,[1,2,7] Ludi Zhang,[2,7,*] Wenming Liu,[2,7] Xiaolong Ma,[2] Jin Cen,[2] Zhen Sun,[2,3] Chenhua Wang,[2] Sisi Feng,[2] Zhengtao Zhang,[2] Liyun Yue,[2] Lulu Sun,[2] Zhenfeng Zhu,[4] Xiaotao Chen,[2] Anqi Feng,[2] Jiaying Wu,[2] Zhiwu Jiang,[5] Peng Li,[5] Xin Cheng,[2] Dong Gao,[2] Luying Peng,[1,*] and Lijian Hui[2,3,6,8,*]

[1]Key Laboratory of Arrhythmias, Ministry of Education, Shanghai East Hospital, Tongji University School of Medicine, Shanghai 200120, China
[2]State Key Laboratory of Cell Biology, Shanghai Institute of Biochemistry and Cell Biology, Shanghai Institutes for Biological Sciences, Chinese Academy of Sciences, University of Chinese Academy of Sciences, Shanghai 200031, China
[3]School of Life Science and Technology, Shanghai Tech University, Shanghai 201210, China
[4]Department of Integrative Oncology, Fudan University Shanghai Cancer Center, Department of Oncology, Shanghai Medical College, Fudan University, Shanghai 200032, China
[5]Key Laboratory of Regenerative Biology, South China Institute for Stem Cell Biology and Regenerative Medicine, Guangzhou Institutes of Biomedicine and Health, Chinese Academy of Sciences, Guangzhou 510530, China
[6]Stem Cell and Regenerative Medicine Innovation Academy, Beijing 100101, China
[7]These authors contributed equally
[8]Lead Contact
*Correspondence: zhangludi@sibcb.ac.cn (L.Z.), luyingpeng@tongji.edu.cn (L.P.), ljhui@sibcb.ac.cn (L.H.)
https://doi.org/10.1016/j.stem.2018.10.018

SUMMARY

Transplantation of human hepatocytes (HHs) holds significant potential for treating liver diseases. However, the supply of transplantable HHs is severely constrained by limited donor availability and compromised capacity for *in vitro* expansion. In response to chronic injury, some HHs are reprogrammed into proliferative cells that express both hepatocyte and progenitor markers, suggesting exploitable strategies for expanding HHs *in vitro*. Here, we report defined medium conditions that allow 10,000-fold expansion of HHs. These proliferating HHs are bi-phenotypic, partially retaining hepatic features while gaining expression of progenitor-associated genes. Importantly, these cells engraft into injured mouse liver at a level comparable to primary HHs, and they undergo maturation following transplantation *in vivo* or differentiation *in vitro*. Thus, this study provides a protocol that enables large-scale expansion of transplantable HHs, which could be further developed for modeling and treating human liver disease.

INTRODUCTION

One remarkable feature of the liver is its outstanding capacity to regenerate after injury. For late-stage liver diseases in which the liver loses its regeneration capability, the only curative therapy is liver transplantation (Dhawan et al., 2010). However, the actual use of liver transplantation is limited due to organ shortages. Transplantation of primary hepatocytes has been evaluated as an alternative to organ transplantation both in clinics and animal models (Dhawan et al., 2010). Human hepatocytes (HHs) with efficient liver repopulation capability are in great demand for liver disease treatment. However, the actual use of hepatocyte transplantation has been hampered by the limited availability of donor hepatocytes and the inability to expand primary HHs (PHHs) *in vitro*.

For decades, expandable HHs have been a bottleneck for their applications for research purposes and clinical therapies (Bhatia et al., 2014; Michalopoulos, 2014; Mitaka, 1998; Runge et al., 2000). Human hepatocyte-like cells (HLCs) have been generated from human pluripotent stem cells by *in vitro* differentiation or from human somatic cells by direct transdifferentiation (Ji et al., 2013). This method was able to generate large numbers of functional HLCs capable of rescuing liver failure in mice after transplantation. Nevertheless, human HLCs showed limited engraftment capability in mouse livers (Gao et al., 2017; Ji et al., 2013). The repopulation efficiency of HLCs, which is around 2%, is far lower than that of PHHs, which is around 70% (Ji et al., 2013; Rezvani et al., 2016; Sampaziotis et al., 2015). Because about 10% of liver cells must be replaced to have therapeutic effect on human patients (Dhawan et al., 2010), further optimization is needed to make these cells compatible with clinical transplantation.

Some efforts have been made to reveal the mechanism of liver regeneration and to translate these findings to improve HH cultures (Kang et al., 2012). The oxygenated or microfabricated co-cultures have been reported to allow HHs to retain metabolic function for a few weeks; however, these cells lose their proliferative capacity (Khetani and Bhatia, 2008; Kidambi et al., 2009). Another study using high-throughput screening identified small molecules that supported HHs for one week with about 10-fold expansion (Shan et al., 2013). Moreover, human liver organoids generated from bile-duct-derived bipotential cells could be expanded long term *in vitro* (Huch et al., 2015). Nevertheless, cells from these expandable organoids show poor performance in transplantation (Huch et al., 2015). In other studies, effort was made to expand HHs by immortalization with hTERT and viral genes, such as SV40, E6, and E7 (Kobayashi et al., 2000; Levy

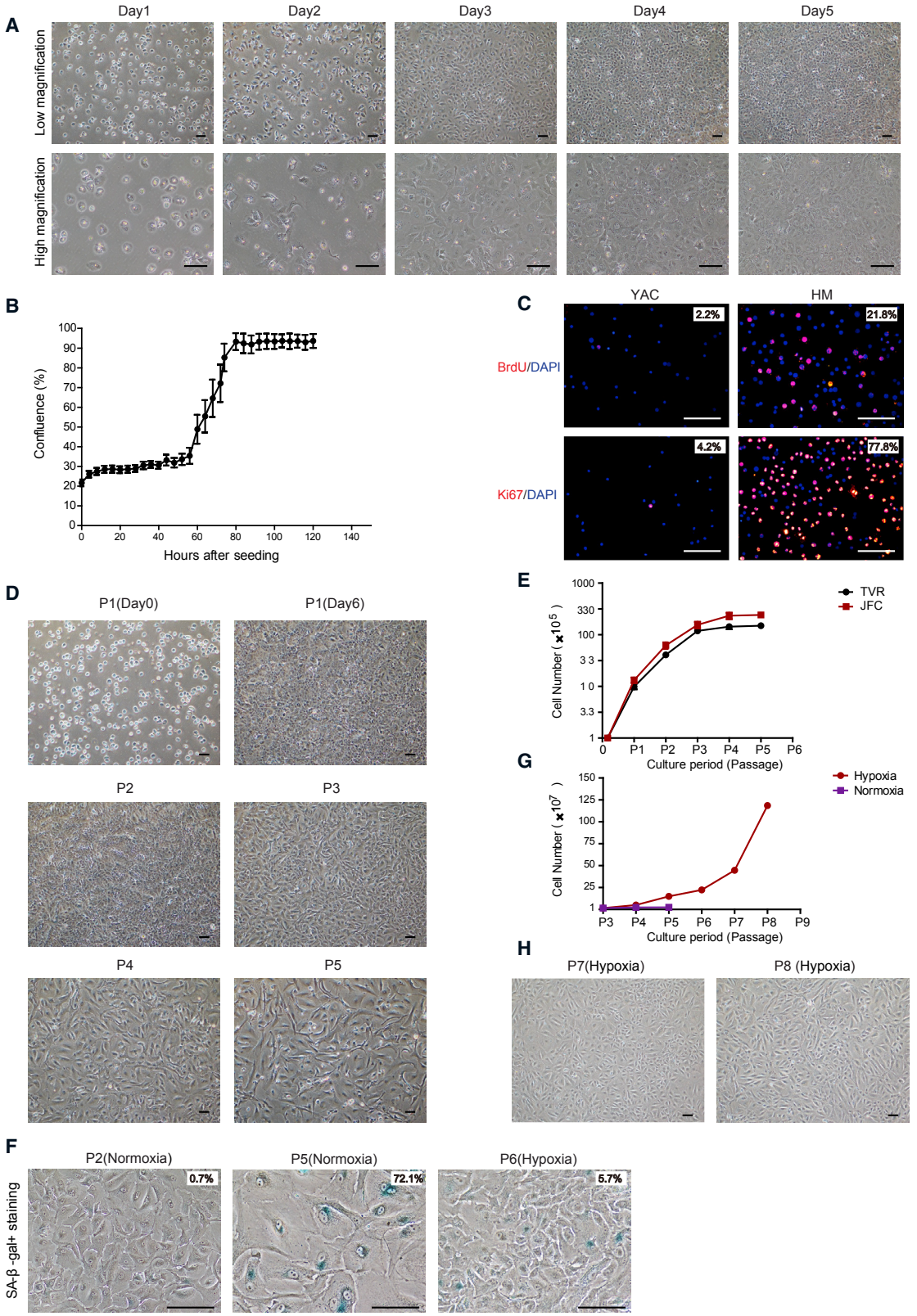

Figure 1. HHs Are Proliferative in HM

(A) Time-lapse images of cultured human hepatocytes (HHs) (lot: JFC) for 5 days in HM. Scale bars, 200 μm.

(B) Time-lapse cell confluence was analyzed by the incuCyte FLR for 5 days in HM.

(legend continued on next page)

et al., 2015). However, no *in vivo* repopulation was demonstrated using cells thus obtained, and overexpression of hTERT and viral oncogenes hold a risk of tumorigenesis after transplantation.

Cell plasticity has lately been recognized to play an important role in liver regeneration (Kopp et al., 2016; Li et al., 2016; Michalopoulos and Khan, 2015). Specifically, during injury, mouse hepatocytes can be reprogrammed to proliferative biliary-like progenitor cells (HepPDs) (Tarlow et al., 2014; Yanger et al., 2013), which lose hepatic features but display the characteristics of liver progenitors (Tarlow et al., 2014). Hepatocyte-to-HepPD conversion is likely to take place through a bi-phenotypic "intermediate" status characterized by the co-expression of hepatocyte markers and progenitor-associated markers (Tanimizu et al., 2014; Yanger et al., 2013). Two recent studies have respectively demonstrated the generation of expandable progenitor-like cells and duct-like cells from rodent hepatocytes *in vitro* (Katsuda et al., 2017; Wu et al., 2017). Despite the cessation of expression of hepatocyte genes *in vitro*, these cells could extensively repopulate mouse livers and regain features of mature hepatocytes, indicating that this may be a means of producing transplantable hepatocytes on a large scale (Katsuda et al., 2017; Wu et al., 2017). Notably, in chronic liver diseases, HHs with expression of progenitor-associated markers were also documented in regenerative nodules (Michalopoulos and Khan, 2015; Yoon et al., 2011), indicating this may be a suitable strategy for expanding HHs at the "intermediate" status *in vitro*.

Here, we developed a defined medium to promote the proliferation of HHs. In combination with hypoxia culture, HHs can proliferate continually for more than one month with 10,000-fold expansion in numbers. Notably, proliferating HHs (ProliHHs) were identified as bi-phenotypic cells, which retained some of the features of mature hepatocytes and expressed progenitor-associated markers. These cells differ from proliferating rodent hepatocytes, which are progenitor-like cells without any hepatic features. ProliHHs can revert back to the status similar to mature hepatocytes. Importantly, these cells substantially repopulated Fah-deficient mouse livers. These findings indicate that human-hepatocyte-derived bi-phenotypic cells are highly proliferative cells with potent capacity for repopulation.

RESULTS

Establishing a Culture System to Induce ProliHHs

We designed the study by first identifying a basic medium for optimizing hepatocyte culture and then modifying this medium for hepatocyte expansion. In total, 10 different media from previous studies and commercial sources were used in the study (see STAR Methods). Cryopreserved human hepatocytes that were 99.9% ALB positive and 100% CK19 negative (Figures S1A and S1B) were seeded at a density of 80% (Figure S1C). To assess the maintenance effect of different media, we documented morphologies and gene expression levels in HHs after culture for 7 days. Among the 10 media, human liver isolation medium (HLIM), hepatocyte growth medium (HGM), and modified minimum Eagles' medium α (MEMa) allowed HHs to maintain their morphology to the most pronounced extent (Figure S1D), and HLIM preserved significantly high levels of mature hepatocyte genes, such as ALB, TTR, and CYP3A4 when compared to freshly thawed human hepatocytes (Figure S1E). HLIM also induced proliferation of HHs at the first passage. By contrast, the rodent hepatocyte medium containing Y-27632, A-83-01, and CHIR99021 (YAC) medium, which was reported to induce the proliferation of rodent hepatocytes (Katsuda et al., 2017), had no effect on HH proliferation. However, HHs quickly lost the features of mature hepatocytes after passage in HLIM, as demonstrated by decreased expression of ALB and HNF4A and morphologic change (Figures S1F and S1G). When HLIM-cultured cells were transplanted to Fah-deficient mice, they showed poor capability to engraft into the liver (Figures S1H and S1I).

We decided to modify HLIM and speculated that key components in the HLIM, such as Wnt3a, Rspo1, Noggin, and forskolin, might not be optimized for the culture of HHs. Notably, removal of Wnt3a-conditioned medium reduced the proliferation of HHs dramatically (Figures S2A and S2B). Removal of Rspo1 or Noggin did not affect the proliferation of hepatocytes but did increase ALB expression (Figures S2A–S2C). When Rspo1, Noggin, and forskolin were removed from HLIM, the new medium strikingly improved proliferation and hepatic gene expression in HHs (Figures S2A–S2C). These findings indicated that Wnt3a is critical in the medium. Indeed, the Wnt pathway was activated to a considerable extent, as indicated by upregulation of AXIN2, DKK1, and LGR5 (Figure S2D). A purified Wnt3a recombinant protein could efficiently replace the Wnt3a-conditioned medium for expansion of HHs and maintenance of the hepatic gene expression (Figures S2E–S2G). However, CHIR99021, a highly selective GSK3β inhibitor, did not facilitate the expansion of HHs (Figure S2H). We defined the HLIM with removal of Rspo1, Noggin, and forskolin as human hepatocyte medium (HM) for expansion of HHs.

ProliHHs Partially Maintain Features of Hepatocytes

After culture in HM, PHHs started to proliferate on day 2 (Figures 1A and 1B; Video S1). We found 77.8% ± 4.1% of the cells were Ki67 positive, and a bromodeoxyuridine (BrdU) pulse labeling for 3 hr showed that 21.8% ± 4.8% of the cells were at the S phase on day 3 (Figure 1C). Notably, HHs from two individuals cultured in HM could be serially passaged for one month with nearly

(C) The proliferation of HHs was determined by BrdU and Ki67 staining on day 3 in HM. Cells were incubated with BrdU for 3 hr. YAC medium was used as a control. BrdU and Ki67-positive cells were quantified. Scale bars, 100 μm.
(D) Images of cultured HHs at five passages in HM under normoxia. Scale bars, 200 μm.
(E) Growth curves of cultured HHs from two individuals were analyzed at indicated passages in HM.
(F) SA-β-gal staining showed increased senescence under normoxia and reduced senescence under hypoxia. SA-β-gal-positive cells were quantified. Scale bars, 200 μm.
(G) Growth curves of cultured HHs under hypoxia and normoxia were analyzed at indicated passages.
(H) Images of cultured HHs at P7 and P8 under hypoxia. Scale bars, 200 μm.
All data are shown as the mean ± SD of three independent experiments. See also Figures S1, S2, and S3.

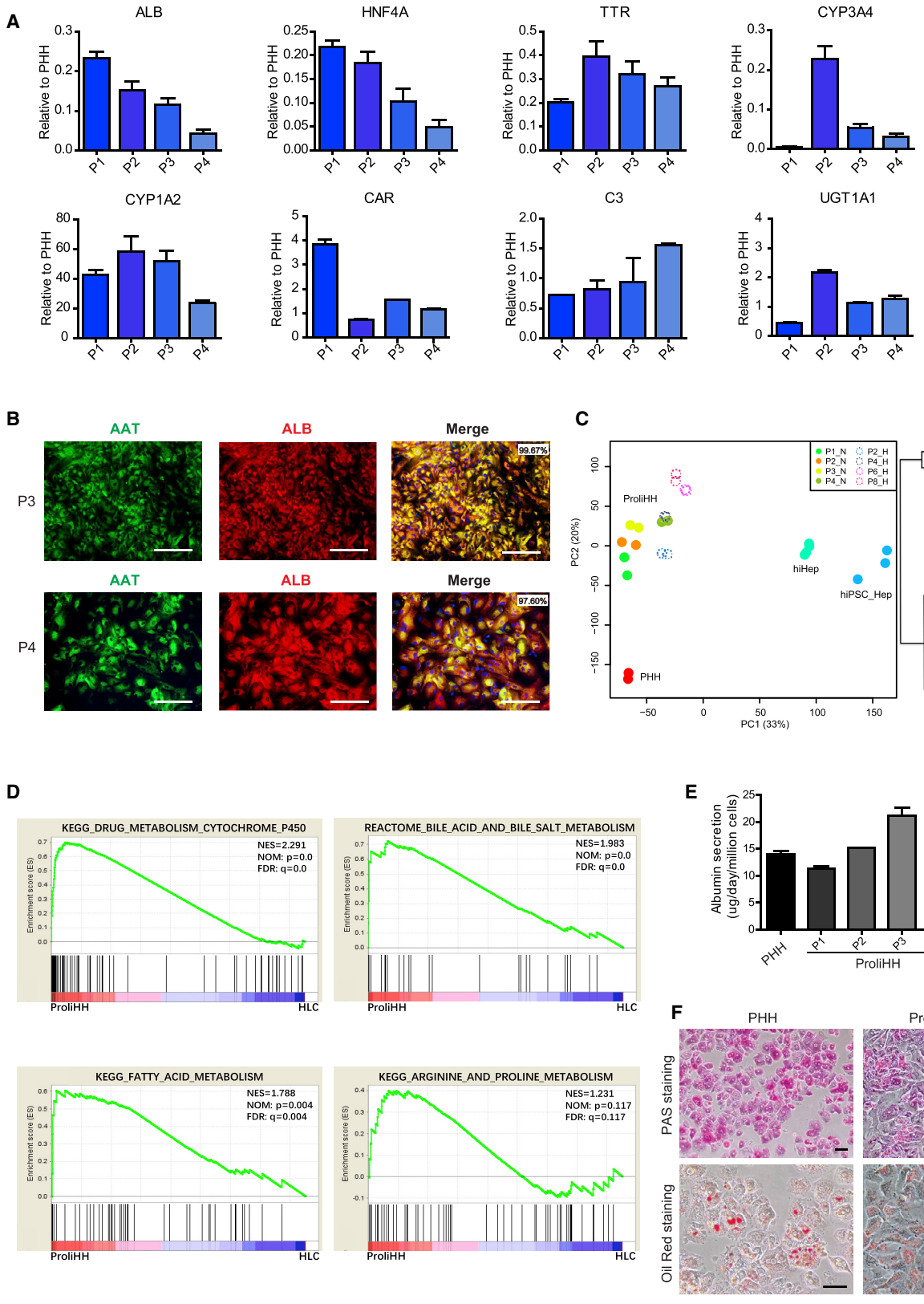

Figure 2. ProliHHs Partially Maintain Mature Hepatic Features

(A) Hepatic gene expressions of ProliHHs at indicated passages under normoxia were measured by qPCR. Data are normalized to freshly thawed primary human hepatocytes (PHHs).

(legend continued on next page)

300-fold expansion in numbers (Figures 1D and 1E). HHs cultured in HM stopped proliferation after 4 passages (Figure 1E). We found that the levels of expression of cell cycle arrest genes and senescence genes increased markedly during the culture (Figure S3A). SA-β-gal staining confirmed the occurrence of senescence, which may explain the cessation of proliferation of HHs (Figure 1F). Because hypoxia has been reported to prevent cultured cells from senescing (Leontieva et al., 2012; Parinello, 2003), we applied HM-cultured HHs in a hypoxic condition of 5% O_2. Markedly, hypoxia culture extended HH proliferation for 4 additional passages (Figures 1G and 1H). HHs cultured under hypoxic conditions showed reduced expression of cell cycle arrest genes and senescence genes and decreased number of SA-β-gal-positive cells (Figures S3B and 1F). HHs under hypoxia conditions showed about 10,000-fold expansion in total number (Figure 1G).

We next assessed hepatic gene expression and hepatic functions of HM-cultured ProliHHs in normoxia. Mature hepatocyte genes were expressed in ProliHHs but at different levels from freshly thawed PHHs. ALB, HNF4A, TTR, and CYP3A4 were expressed at lower levels, and CYP1A2, CAR, C3, and UGT1A1 were at similar levels or higher (Figure 2A). The expression of ALB and AAT proteins was validated by immunofluorescent staining, showing that over 97% of ProliHHs were positive for both ALB and AAT at passage 3 (P3) and P4 (Figures 2B and S3C). These data were different from expandable rodent hepatocytes (Katsuda et al., 2017; Wu et al., 2017), which showed almost undetectable expression of hepatocyte genes. It is noteworthy that ProliHHs expressed hepatic genes at comparable levels under normoxia and hypoxia (Figures S3D and S3E). Interestingly, HHs lost tetraploidy and shifted to diploidy during the expansion, showing 67% at tetraploidy and 28.6% at diploidy in freshly thawed PHHs and 8% at tetraploidy and 88% at diploidy in ProliHHs (Figure S3F).

We further compared the global gene expression between freshly thawed PHHs and ProliHHs cultured in normoxia by RNA sequencing analysis. To verify the extent to which ProliHHs maintained hepatic gene expression, we used HLCs derived from human pluripotent stem cells (hiPSC-Hep) or from human somatic cells by direct transdifferentiation (hiHep) as controls (Gao et al., 2017). Notably, principal-component analysis (PCA) and hierarchical clustering revealed that ProliHHs formed an associated group and were distinct from other cells (Figures 2C and S4A). Nevertheless, ProliHHs clustered closely with PHHs but remained distantly from HLCs (Figure 2C). Moreover, ProliHHs showed enrichment in expression of genes involved in fatty acid and drug metabolism (Figures 2D, S4B, and S4C). These data suggested that hepatic function genes were retained in ProliHHs. In line with the hepatic gene expression, HM-cultured ProliHHs displayed some of the functions of mature hepatocytes, such as albumin secretion, glycogen storage, and cytoplasmic accumulation of lipids (Figures 2E and 2F). Intriguingly, when hypoxia-cultured ProliHHs were included into the analysis, we found that, although all ProliHHs were grouped together (Figure 2C), hypoxia-cultured ProliHHs at late passages (after P6) shifted from the main cluster and showed an attenuated hepatic phenotype (Figure 2C). These results indicated that ProliHHs maintain some characteristics of mature hepatocytes.

ProliHHs Are at a Bi-phenotypic Status

We next examined whether ProliHHs might gain features of progenitor cells. Notably, ProliHHs showed increased expression of progenitor-associated signature genes that were upregulated during the conversion from human hepatocytes to HepPD cells, such as SOX9, CD133, EPCAM, CD44, CK19, and CK7 (Tarlow et al., 2014; Figures 3A and S4D). Immunofluorescent staining of SOX9, CK19, and CK7 indicated that almost all ProliHHs at P4 or later passages were positive for the three markers (96.95%, 99.07%, and 99.24%, respectively; Figures 3B and S4E), and flow cytometry analysis confirmed that 98% of ProliHHs were CD133-positive (Figure S4F). Notably, ProliHHs did not express hepatoblast marker α-fetoprotein (AFP), suggesting that these cells are not likely to act as fetal hepatoblasts in HM culture (Figure S4G). Moreover, functional genes for mature bile ducts, such as cystic fibrosis transmembrane conductance regulator (CFTR), secretin receptor (SCTR), somatostatin receptor 2 (SSTR2), and aquaporin-1 (AQP1), were not expressed in ProliHHs (Figure S4H), indicating that ProliHHs were not mature bile duct cells.

Because no expression profile of human HepPDs or human liver progenitor cells is available, we used hiPSC-derived liver progenitor-like cells (LPCs) (Shih et al., 2015) to assess the similarity between normoxia-cultured ProliHHs and LPCs. When compared to PHHs, 3,482 genes were significantly upregulated in LPCs, among which 1,652 (47.4%) were also upregulated in ProliHHs (Figure 3C). Based on the pattern of differential gene expression between PHHs, ProliHHs, and LPCs, the LPC-enriched genes could be divided into three clusters (Figure 3D). Notably, gene set enrichment analysis (GSEA) confirmed that genes in cluster I and II were enriched in several pathways relative to stem cells and cell cycles (Figure 3E), suggesting the acquisition of progenitor-associated features in ProliHHs during the passage. Cluster III genes, such as the previously reported

(B) The expression of ALB and AAT of ProliHHs under normoxia was determined by co-immunofluorescent staining. The percentages of ALB and AAT double-positive cells were quantified. Scale bars, 100 μm.

(C) Principal-component analysis was performed to compare global gene expression profiles in ProliHHs (P1, P2, P3, and P4 under normoxia; P2, P4, P6, and P8 under hypoxia), PHH, hiHep, and hiPSC-Hep. Normoxia and hypoxia was represented in the diagram as N and H, respectively. Left: a scatterplot of the expression profiles on the planes spanned by the first and second principal components (PCs) is shown. Right: a dendrogram of the hierarchical clustering of expression profiles is shown.

(D) Gene set enrichment analysis (GSEA) was performed to identify enriched pathways between ProliHHs under normoxia and HLCs.

(E) The human albumin secretion of ProliHHs in different passages under normoxia was measured by human albumin ELISA.

(F) Glycogen storage and lipid accumulation in ProliHHs at P4 under normoxia was analyzed by periodic acid-Schiff (PAS) staining and oil red O staining, respectively. Scale bars, 100 μm.

See also Figure S4.

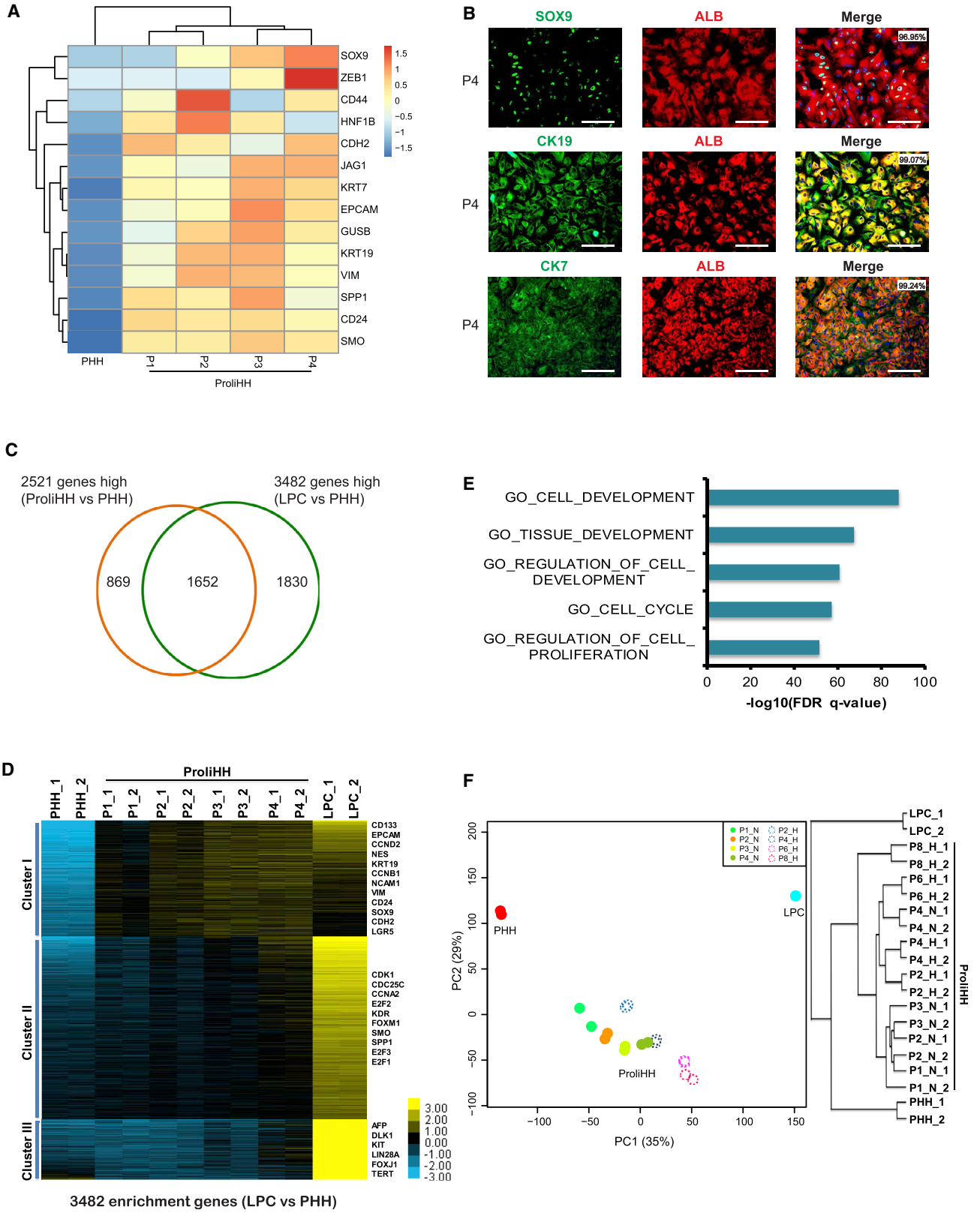

(legend on next page)

progenitor-associated markers DLK1, KIT, and FOXJ1 (Miyajima et al., 2014), were not fully upregulated in ProliHHs (Figure 3D). Intriguingly, when whole expression profiles were analyzed, ProliHHs cultured in normoxia still clustered close to PHHs and were separated from LPCs (Figure 3F). Previous studies revealed functions of Wnt and Yap pathways in promoting hepatocyte-to-progenitor reprogramming *in vivo* (Tarlow et al., 2014; Yimlamai et al., 2014). In line with these findings, we found that Wnt target genes and conserved YAP signature genes were enriched in ProliHHs (Figure S4I), suggesting possible mechanistic roles of Wnt and Yap in conversion of HHs to ProliHHs. Notably, when expression profiles of hypoxia-cultured ProliHHs were characterized, we found that ProliHHs at late passages showed a tendency to express progenitor-like profiles (Figure 3F). These results collectively suggested that, although ProliHHs yet not established the whole gene profile of progenitor cells, they expressed a large portion of LPC genes. ProliHHs were rather at a bi-phenotypic "intermediate" status between mature hepatocytes and liver progenitor cells.

ProliHHs Are Revertible to Mature Status

We next investigated whether ProliHHs are plastic and can re-acquire mature hepatocyte characteristics. To that end, we took confluent ProliHHs at early (before P4) and late (after P6) passages and cultured them in hepatocyte maturation medium for 10 days in a three-dimensional culture (Figure 4A; Bell et al., 2016; Huch et al., 2015). Under the maturation condition, ProliHHs formed typical morphology of mature hepatocytes and showed polygonal shape (Figures 4B and 4C). Notably, some cells showed bi-nuclei that were not detected in HM-cultured ProliHHs (Figure 4B). Hepatocyte genes, such as ALB, TTR, HNF4A, and AAT, were significantly increased in ProliHHs after maturation (Figure 4D). In concordance with increased mRNA levels in genes involved in CYP2B6 metabolism and urea synthesis, the metabolic activity of CYP2B6 and the capacity for urea synthesis were induced in ProliHHs after maturation (Figures 4E and 4F). By contrast, the expression levels of progenitor-associated genes, such as SOX9, CK19, and CK7, were largely reduced as shown by the qPCR (Figure 4G). Immunofluorescent staining of ALB, CK19, and CK7 validated the qPCR data and showed no formation of mature bile duct cells (Figures 4G and S4J). Together, these results suggest that ProliHHs could be reverted to a status close to that of mature hepatocytes.

ProliHHs Generated from Multiple Individuals

We then applied the protocol to generate ProliHHs from hepatocytes of 10 additional individuals (see STAR Methods for detailed information). Notably, hepatocytes of 7 additionally tested individuals of different sex, age, and race could be expanded for at least 5 passages in HM. Interestingly, cells from the 5 young donors at ages <11 years showed 1,000- to 10,000-fold expansion in total number at P8, whereas hepatocytes from 2 of 5 adult donors at ages >37 years could be expanded about 1,000-fold in cell number at P5 and showed the cumulative growth curve similar to that of young donor cells (Figures S5A–S5C). These data suggested that hepatocytes from young individuals appeared to possess high capability to proliferate in the HM medium. ProliHHs derived from the new donors were bi-phenotypic, showing partial retention of hepatocyte-specific genes and functions (Figures S5D–S5G) alongside the gained expression of progenitor-associated genes (Figures S5D and S5E). Moreover, upon differentiation in the HIM medium, proliHHs displayed enhanced functions of mature hepatocytes, such as the CYP2B6 activity (Figures S5H and S5I). These results indicated that HM could be used to expand HHs from genetically diversified individuals.

ProliHHs Efficiently Engraft into Mouse Livers after Transplantation

We next examined the *in vivo* repopulation of ProliHHs by transplanting them into immune-deficient *Fah*$^{-/-}$ mice (*Fah*$^{-/-}$*Rag2*$^{-/-}$*IL2rg*$^{-/-}$ [FRG]), a model of human tyrosinemia type I (Grompe et al., 1993). FRG mice die from liver failure unless they are supplied with 2-(2-nitro-4-trifluoro-methylbenzyol)-1,3-cyclohexanedione (NTBC) or transplanted with primary hepatocytes after NTBC withdrawal (Azuma et al., 2007). Transplantation to FRG mice thus provides a useful model to characterize the *in vivo* function of ProliHHs.

All FRG mice without hepatocyte transplantation died within 4 months, whereas 5 of the 7 FRG mice survived after receiving PHH transplantation (Figure 5A). Notably, 11 of the 14 FRG mice that transplanted with ProliHHs at early passages (before P4) survived for more than 4 months (Figure 5A), showing similar survival curve with PHH-transplanted FRG mice (log rank test; $p = 0.72$). The ProliHH-transplanted mice lost body weight during the first 4 weeks after transplantation but later regained the body weight and remained stable, suggesting that transplanted ProliHHs restored functions of the diseased *Fah*$^{-/-}$ livers (Figure 5B). The mice that underwent ProliHH transplantation gained body weight one week later than mice transplanted with PHHs (Figure 5B), suggesting that ProliHHs may require additional time to support liver function after transplantation.

Serum levels of aspartate transaminase (ALT), alanine transaminase (AST), and total bilirubin (TBIL) were significantly

Figure 3. ProliHHs Are Bi-phenotypical Cells

(A) The expression of HepPD signature genes in ProliHHs in normoxia and freshly thawed PHH based on RNA-seq data.

(B) The co-expression of the mature hepatic marker ALB and progenitor-associated markers, such as SOX9, CK19, and CK7, was determined by immunofluorescent staining in ProliHHs at P4. The percentages of ALB$^+$SOX9$^+$, ALB$^+$CK19$^+$, and ALB$^+$CK7$^+$ cells were quantified. Scale bars, 100 μm.

(C) Venn diagram for upregulated genes (fold change ≥ 3) in ProliHHs and LPCs when compared to PHH.

(D) Hierarchical clustering was performed for LPC-enriched genes between PHH, ProliHHs, and LPCs.

(E) GSEA was performed to identify enriched pathways in clusters I and II.

(F) Principal-component analysis was performed to compare global gene expression profiles in ProliHHs (P1, P2, P3, and P4 under normoxia; P2, P4, P6, and P8 under hypoxia), PHH, and LPCs. Normoxia and hypoxia was represented in the diagram as N and H, respectively. Left: a scatterplot of the expression profiles on the planes spanned by the first and second principal components (PCs) is shown. Right: a dendrogram of the hierarchical clustering of expression profiles is shown.

See also Figure S4.

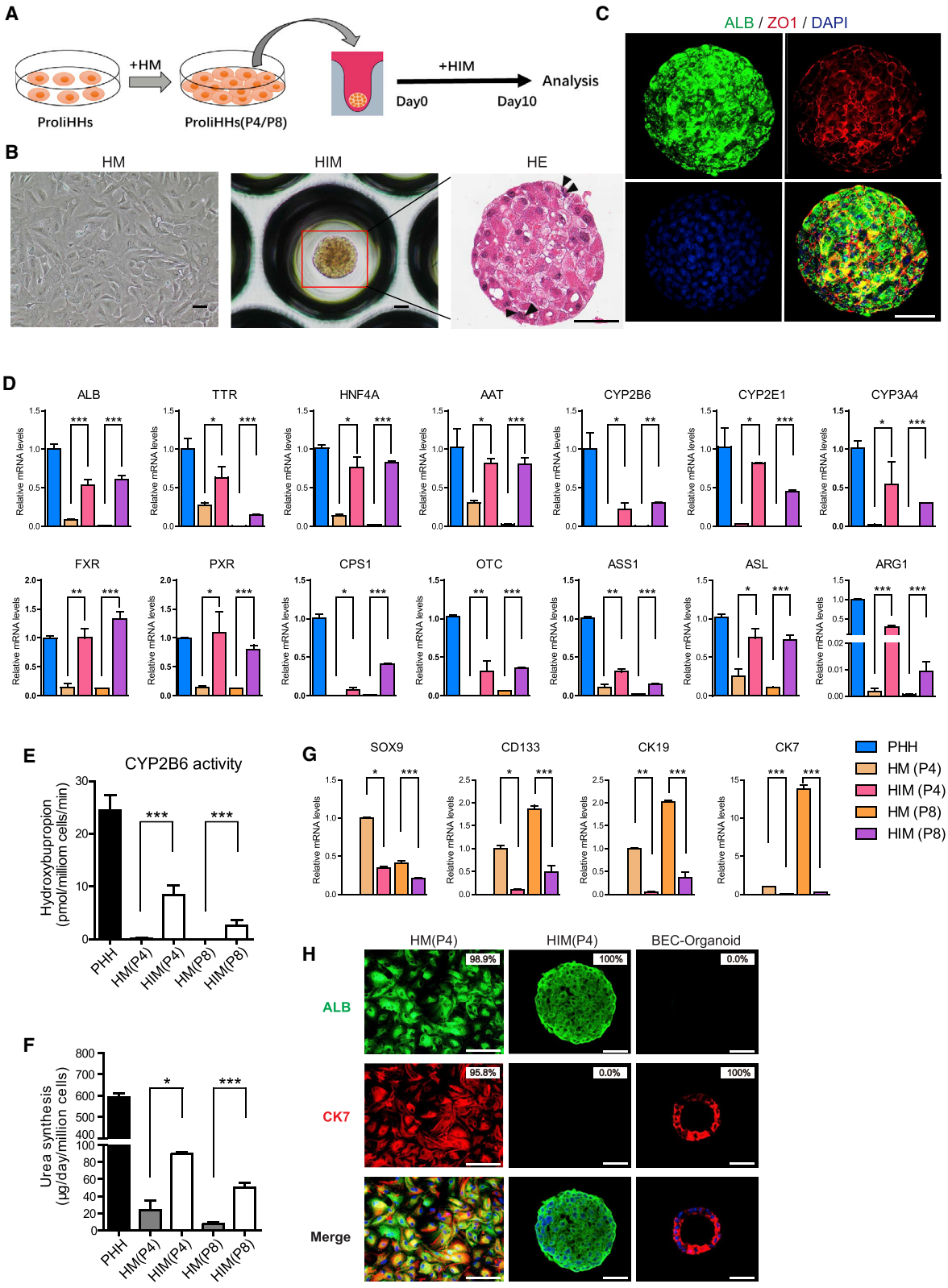

Figure 4. ProliHHs Revert Back to Mature Features *In Vitro*

(A) Schematic of hepatic induction. ProliHHs were cultured in HM for expansion. Confluent hypoxia-cultured ProliHHs at P4 and P8 were induced to form 3D organoids in HIM for hepatic maturation.

(legend continued on next page)

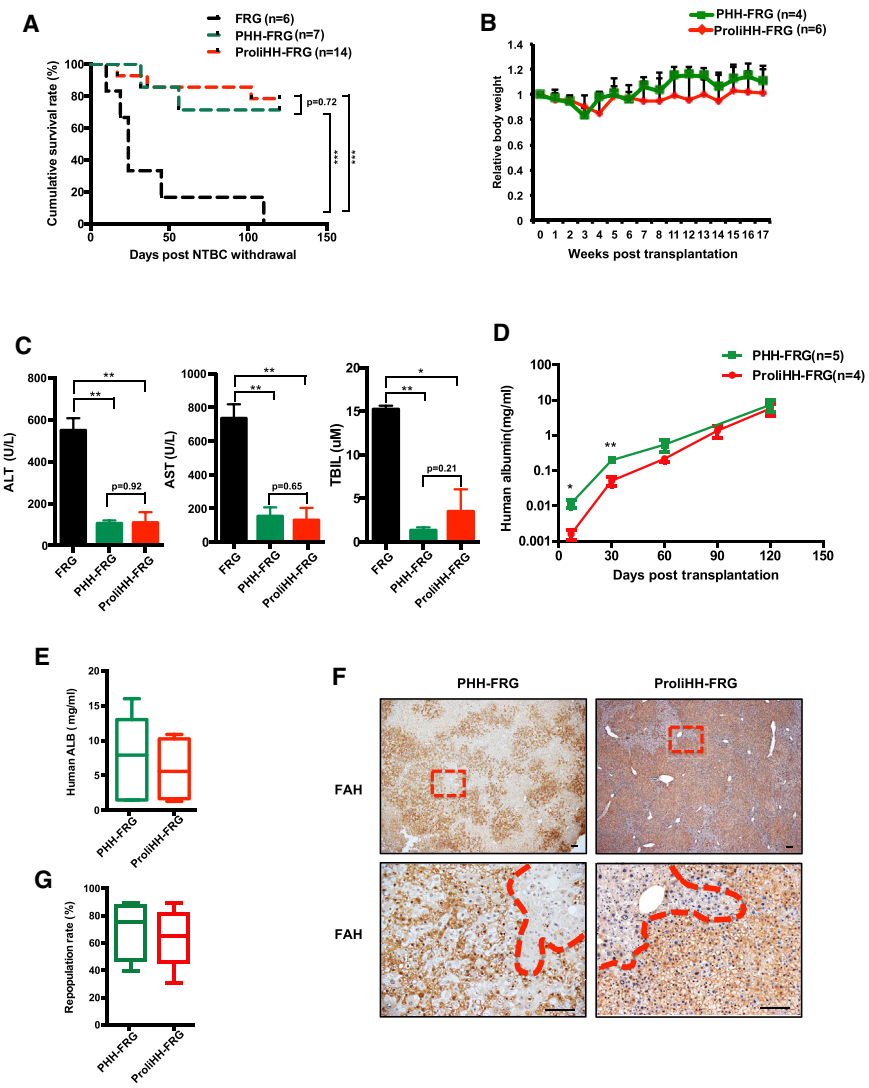

Figure 5. ProliHHs Robustly Repopulate in Mouse Livers

(A) Kaplan-Meier survival curve of FRG mice without transplantation and with transplantation of 5×10^5 ProliHHs at early passages (ProliHH-FRG) or PHHs (PHH-FRG).

(B) The body weight changes of ProliHH-FRG mice and PHH-FRG mice.

(C) Serum levels of ALT, AST, and TBIL in moribund control FRG mice (n = 3), survived ProliHH-FRG mice (n = 4), and survived PHH-FRG mice (n = 3).

(D) The dynamic process of human ALB levels was determined by ELISA in the survived ProliHH-FRG mice and survived PHH-FRG mice during 4 months after transplantation.

(E) The human ALB levels were determined by ELISA in the survived ProliHH-FRG mice (n = 4) and survived PHH-FRG mice (n = 5) 4 months after transplantation.

(F) Immunohistochemical results using Fah antibody in livers of ProliHH-FRG and PHH-FRG mice 4 months after transplantation.

(G) The repopulation efficiency of ProliHHs (n = 4) and PHHs (n = 5) in mice was determined by Fah immunostaining 4 months after transplantation.

Scale bars, 100 μm. The data are shown as the mean ± SD. **p < 0.01; ***p < 0.001; log rank test for (A) and Student's t test for (B)–(G). See also Figure S6.

reduced in both PHH-transplanted and ProliHH-transplanted FRG mice (no significance between PHH and ProliHH), further confirming the improved liver functions in these mice (Figure 5C). The secretion of human albumin in mouse serum increased gradually after transplantation of ProliHHs (Figure 5D) and reached the levels of 5.8 ± 4.5 mg/mL at 4 months, which were comparable to mice receiving PHHs (7.3 ± 6.1 mg/mL; p = 0.69; Figure 5E). Moreover, when ProliHHs from other donors were transplanted, we found that human albumin levels could reach the comparable scope (around 0.1–1 mg/mL at 3 months after transplantation) in FRG-recipient mice (Figure S6A). Notably, serum albumin levels in mice transplanted with PHHs were higher than in mice transplanted with ProliHHs during the first 3 months after transplantation (Figure 5D), again suggesting that ProliHHs may require more time to restore liver functions.

To analyze the repopulation efficiency of ProliHHs, we harvested liver samples at 4 months after transplantation. Immunohistochemical staining of Fah showed that ProliHHs repopulated 64% ± 21.8% of the liver parenchyma in the survived mice (Figures 5F and 5G). This repopulation efficiency was comparable to that of primary hepatocytes (70.4% ± 21.5%; p = 0.66; Figures 5F and 5G). The engraftment of ProliHHs in recipient livers was further demonstrated by genomic PCR for human-specific Alu DNA sequence (Figure S6B). Notably, repopulated ProliHHs,

(B) Representative images of the ProliHHs without hepatic induction and ProliHH-derived 3D organoids after hepatic induction. Black arrows indicated the bi-nuclei cells. Scale bars, 100 μm.

(C) The co-immunofluorescent staining of ALB and ZO1 in ProliHH-derived 3D organoids. Scale bars, 100 μm.

(D) Expression of hepatocyte genes was determined by qPCR after 10-day induction in HIM. Data are normalized to freshly thawed PHH.

(E) The metabolic products of hydroxybupropion (assay for CYP2B6 activity) were determined by liquid chromatography-tandem mass spectrometry. Freshly thawed PHHs were directly used as a positive control.

(F) Urea synthesis after hepatic induction was measured. Freshly thawed PHHs were directly used as a positive control.

(G) Expression of progenitor-associated genes was determined by qPCR after 10-day induction in HIM. Data are normalized to ProliHHs at P4 in HM.

(H) The expression of ALB and CK7 in ProliHHs at P4 and ProliHH-derived 3D organoids was determined by immunofluorescent staining. Biliary epithelial cell (BEC)-derived organoids were used as a positive control. The percentages of ALB- and CK7-positive cells were quantified. Scale bars, 100 μm.

The data are shown as the mean ± SD. *p < 0.05; **p < 0.01; ***p < 0.001; Student's t test. See also Figures S4 and S5.

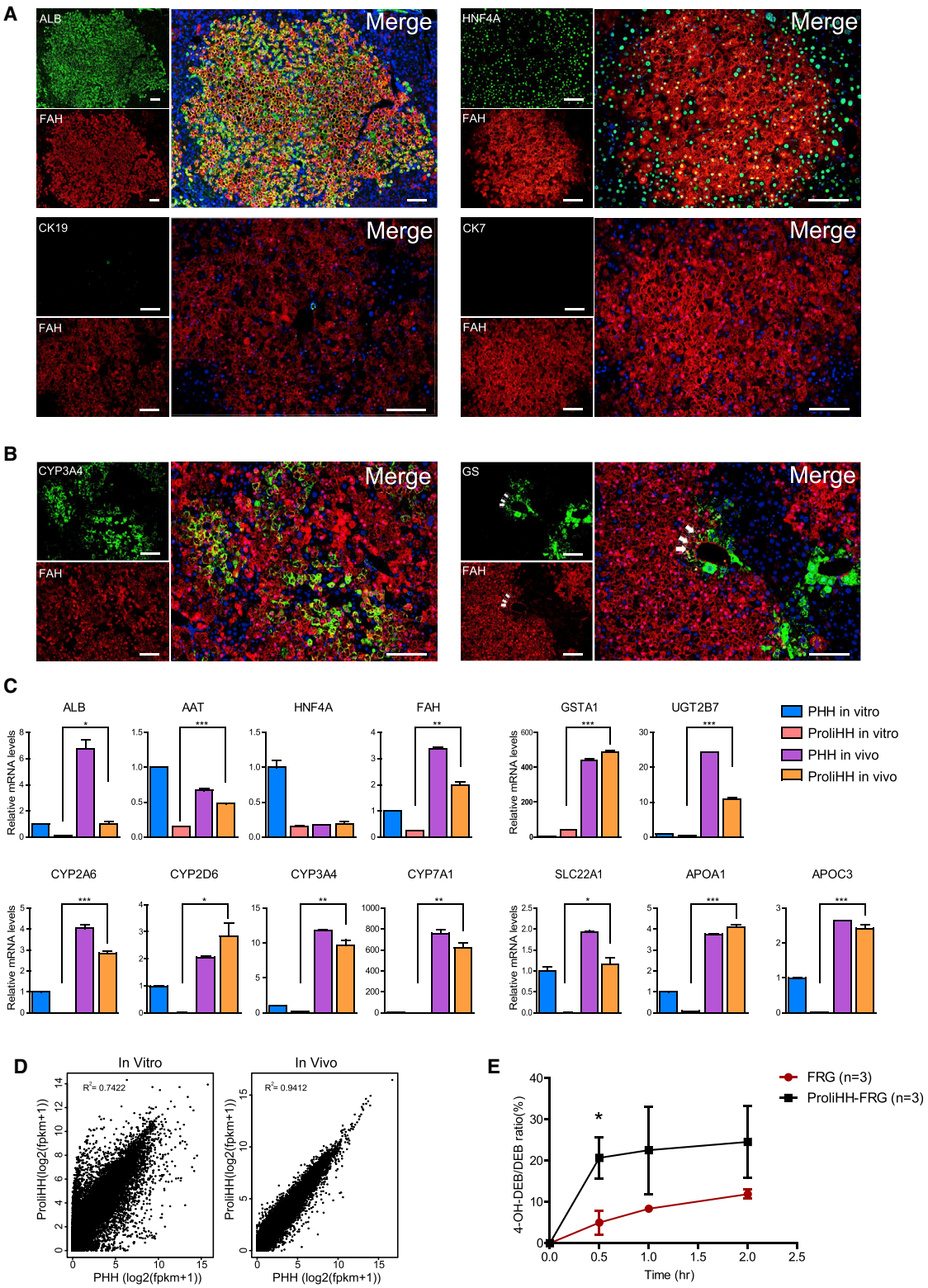

Figure 6. *In Vivo* Maturation of ProliHHs after Transplantation

(A)The maturation of repopulated ProliHHs was analyzed by co-immunofluorescent staining for Fah, ALB, HNF4a, CK19, and CK7.

(B) The liver zonation was analyzed by co-immunofluorescent staining for Fah, CYP3A4, and GS. Arrows depict human hepatocytes positive for hepatic markers GS and Fah.

(legend continued on next page)

which were Fah-positive, could be distinguished from mouse hepatocytes by showing the pale cytoplasm staining of eosin (Figure S6C) and increased accumulation of lipid (Figure S6D). These observations were in consistence with the features of PHH-repopulated liver tissues (Figures S6C and S6D). Importantly, tumors were not found in ProliHH-transplanted FRG mice 4 months after transplantation (Figure S6E). Moreover, ProliHHs did not form tumors after subcutaneous xenograft in immunodeficient mice (Figure S6F). These data suggested that ProliHHs efficiently repopulated FRG liver and had therapeutic effects in treating liver injuries.

Maturation of ProliHHs after Repopulation *In Vivo*

We next characterized whether ProliHHs underwent further maturation *in vivo*. Immunofluorescent staining showed repopulated ProliHHs remained the expression of ALB and HNF4A and ceased expression of CK19 and CK7 (Figure 6A). The pericentral expression of CYP3A4 and GS indicated that liver zonation had been established in repopulated mouse livers (Figure 6B). We also evaluated hepatic gene expression of repopulated ProliHHs by qPCR using human-specific primers. The repopulated ProliHHs showed significantly more expression of mature hepatic genes, including phase I and II enzymes and transporters, at the levels comparable to PHHs after transplantation (Figure 6C). We further performed human-specific RNA sequencing analysis on whole-liver homogenates to evaluate global gene expression patterns in the repopulated ProliHHs. There was a closer correlation between the gene expression profiles of repopulated ProliHHs and repopulated PHHs than between counterparts *in vitro* (*in vivo* $r^2 = 0.94$ versus *in vitro* $r^2 = 0.74$; Figure 6D).

To further assess the maturity of repopulated ProliHHs, we determined whether human-specific drug metabolism could take place in transplanted livers. To that end, we measured a unique metabolism function of human hepatocytes executed by CYP2D6, which converts a prototypical substrate debrisoquine (DEB) to its 4-OH metabolite (4-OH DEB) (Hasegawa et al., 2011; Masubuchi et al., 1997). FRG mice transplanted with ProliHHs showed significantly higher amounts of 4-OH DEB in sera than in the control group (Figure 6E). The DEB metabolism data in ProliHH-transplanted mice were similar to the data reported in liver-humanized mice (Hasegawa et al., 2011). Together, these data suggested that ProliHHs underwent further maturation with human-specific metabolism *in vivo*.

Finally, we transplanted ProliHHs at late passages (after P6) to FRG mice. Serum levels of human albumin were measured to monitor the repopulation of transplanted ProliHHs (Azuma et al., 2007). The serum level of human albumin was steadily increased in FRG mice after transplantation of late-passage ProliHHs (Figure S6G). Interestingly, human albumin levels showed a delayed kinetics when compared with human albumin in mice transplanted with early-passage ProliHHs. Nevertheless, human albumin levels reached a significant level of 1.9 ± 1.2 mg/mL 20 weeks after transplantation, which was in the comparable range of human ALB levels in early passage ProliHH-transplanted mice (Figure S6G). Moreover, immunohistochemical (IHC) staining of the FAH enzyme showed that ProliHHs at late passages could repopulate 29% ± 12% of FRG livers (Figures S6H and S6I). Importantly, we found that the expression of hepatocyte genes, including albumin, AAT, and HNF4a, was markedly increased (Figures S6J and S6K) and the expression of bile duct cell gene CK19 was almost undetectable (Figure S6J) in late-passage ProliHH-repopulated livers. These data suggest that late-passage ProliHHs largely maintain the repopulation capability and could be further matured *in vivo*.

DISCUSSION

Primary human hepatocyte culture has been an unmet need for a long time (Runge et al., 2000). Here, we established an *in vitro* culture protocol to convert HHs to an expandable bi-phenotypic status, which expressed markers of both mature hepatocytes and liver progenitors. Notably, these cells could be serially expanded up to 10,000-fold. The ProliHHs retained some of the functional characteristics of mature hepatocytes, including plasma protein secretion, glycogen storage, and lipid accumulation. These cells were found to mature further in the hepatocyte maturation medium. Importantly, ProliHHs showed the remarkable capability to repopulate around 60% of the liver after *in vivo* transplantation. It is remarkable that, during the passage, some genes related to maturation were significantly reduced and, vice versa, genes related to progenitors were increased, indicating that, as ProliHHs expand in number, their ability to mature is affected. Intriguingly, this is associated with a decreased repopulation of the ProliHHs in FRG livers.

Previous protocols showed about 10-fold expansion of HHs *in vitro* if no genetic modifications were applied (Shan et al., 2013), whereas, in the current protocol, HHs could expand up to 10,000-fold at P8 without any genetic manipulation. Hepatocyte transplantation is a promising alternative treatment to liver transplantation, especially in treating infants and young children with inborn errors of metabolism. The number of viable cells transplanted for one patient is around 10^9 (Dhawan et al., 2010). Following our protocol, one could obtain 10^9 transplantable hepatocytes from commercial primary human hepatocytes (10^7 hepatocytes per vial) by expanding them for about 100-fold within 3 or 4 passages. As a proof of principle, our study provides a protocol for expansion of HHs, which may be further developed as a cellular source for the treatment of liver diseases.

Wnt3a appeared to be essential to the initiation of the proliferation of HHs. Removal of Wnt3a reduced the proliferation of human hepatocytes dramatically. We found the significant upregulation of Wnt target genes in ProliHHs. This is in line with the important function of the Wnt pathway in hepatocyte proliferation (Janda et al., 2017; Wang et al., 2015) and reprogramming

(C) The Comparison of gene expression of mature hepatic markers, such as phase I, phase II enzymes, and transporters genes in PHHs, ProliHHs, repopulated PHHs, and repopulated ProliHHs. RNA was extracted from repopulated livers. Human-specific primers were used in qPCR.

(D) The correlation between the gene expression profiles of ProliHHs and PHHs *in vitro* and *in vivo*.

(E) Human (CYP2D6)-specific drug biotransformation in ProliHH-FRG mice. The serum concentrations of DEB and 4-OH DEB in control FRG mice (n = 3) and ProliHH-FRG mice (n = 3) were measured 0–2 hr after administration of DEB (2 mg/kg).

Scale bars, 100 μm. The data are shown as the mean ± SD. *$p < 0.05$; **$p < 0.01$; ***$p < 0.001$; Student's t test. See also Figure S6.

(Tarlow et al., 2014) during liver regeneration. Interestingly, CHIR99021, a canonical Wnt agonist, could not replace Wnt3a in expanding human hepatocytes. This may be explained by that Wnt3a not only activates the canonical Wnt signaling but also crosstalks with other pathways, such as the Hippo/YAP pathway (Azzolin et al., 2014). Indeed, GSEA analysis revealed that YAP signature genes were enriched in ProliHHs compared to PHHs. Given that the YAP signaling is also important in induction of progenitor expansion in the liver (Yimlamai et al., 2014), it is possible that the Wnt and YAP pathways might possess important functions in induction of ProliHHs *in vitro*.

ProliHHs showed increased expression of cell cycle arrest genes, such as P21 and P53, after culture for around 1 month and ceased proliferation due to cell senescence. It is reported that sustained activation of the Wnt pathway induces a senescence-like phenotype dependent on ARF and p53 (Damalas et al., 2001). However, the link between Wnt3a and senescence needs to be further addressed in the future. Notably, we showed that hypoxia could largely attenuate the senescence. Because it has been reported that hypoxia suppresses P21-induced senescence by inhibition of the mTOR pathway (Leontieva et al., 2012), it is worth determining whether mTOR inhibitors could maintain further long-term expansion of ProliHHs.

Recently, it has been demonstrated that both mouse and human hepatocytes could be reprogrammed to HepPDs *in vivo* following liver injury (Tarlow et al., 2014; Yanger et al., 2013). The proliferating bi-phenotypic cells derived from human hepatocytes *in vitro* in our study may further support the conclusion that human hepatocytes exhibit cell plasticity. Notably, two recent studies demonstrated that small molecules could reprogram rodent hepatocytes to liver progenitor-like cells, which exhibited liver progenitor features at the transcriptional and functional levels. Interestingly, liver progenitor-like cells from the two studies neither expressed any markers of mature hepatocytes, such as ALB or CYP450 genes, nor had the functions of mature hepatocytes, such as glycogen storage (Katsuda et al., 2017; Wu et al., 2017). By contrast, the ProliHHs generated in our study retained the expression of hepatocyte genes and functions, though at levels lower than PHHs. These differences between rodent and human proliferative hepatocytes may present different stages during the hepatocyte-to-progenitor conversion *in vitro* or it may merely reflect the species difference. Importantly, both rat CLiPs and human ProliHHs could efficiently repopulate the diseased liver when transplanted to urokinase-type plasminogen activator (uPA)/severe combined immunodeficiency (SCID) and FRG mice, respectively. However, given the difference in recipient animal models and donor cells, it is difficult to compare the therapeutic effects directly between rat CLiPs and human ProliHHs.

One of the hallmarks of primary human hepatocytes is their remarkable repopulation capacity after transplantation (Rezvani et al., 2016). Human HLCs generated by differentiation or transdifferentiation recapitulate numerous mature hepatocyte phenotypes that are useful for *in vitro* modeling (Du et al., 2014; Huang et al., 2014; Sampaziotis et al., 2015). However, they show limited liver repopulation efficiency (Ji et al., 2013; Rezvani et al., 2016). By contrast, ProliHHs, which also partially maintained the mature phenotypes of hepatocytes, can repopulate injured livers around 60% and further mature *in vivo*, suggesting their potential for liver regenerative therapy. Because for some liver diseases a repopulation of 10% would be sufficient to show therapeutic effect (Dhawan et al., 2010), such repopulation capability of ProliHHs would be of notable value for these clinical indications. Moreover, it would be interesting to further characterize the transcriptomes among PHHs, ProliHHs, and HLCs and identify the key molecular mechanism for cell repopulation.

In conclusion, our protocol for ProliHHs provides insights into HH culture and a source of cells for therapeutic purposes. In addition, ProliHHs can revert back to mature hepatocytes, as evidenced by the elevated expression of mature hepatocyte genes. It may be possible to use these cells for the study of drug metabolism, hepatitis virus infection, and liver disease modeling *in vitro*.

STAR★METHODS

Detailed methods are provided in the online version of this paper and include the following:

- KEY RESOURCES TABLE
- CONTACT FOR REAGENT AND RESOURCE SHARING
- EXPERIMENTAL MODEL AND SUBJECT DETAILS
  - Human hepatocyte culture
  - L-Wnt3a cell culture
  - Mice
- METHOD DETAILS
  - Time-lapse imaging at a low cell density
  - PCR
  - Human Albumin ELISA
  - Urea synthesis assay
  - Histology, immunohistochemistry and immunofluorescence staining
  - Assays for PAS and Oil Red O staining
  - Senescence-Associated β-Galactosidase Analysis
  - CYP metabolism assay
  - Transplantation of cells into $Fah^{-/-}Rag2^{-/-}Il2rg^{-/-}$ mice
  - Tumor formation assay
- QUANTIFICATION AND STATISTICAL ANALYSIS
  - RNA-sequencing data process
  - Pathway enrichment analysis
  - Statistical Analyses
- DATA AND SOFTWARE AVAILABILITY
  - Data Resources

SUPPLEMENTAL INFORMATION

Supplemental information includes six figures, three tables, and one video and can be found with this article online at https://doi.org/10.1016/j.stem.2018.10.018.

ACKNOWLEDGMENTS

We are thankful to Dr. Hans Clevers for the L-Wnt3a cell line. This project is supported by "Strategic Priority Research Program" of the Chinese Academy of Sciences (CAS) (XDA16020201), Shanghai Science and Technology Committee (16JC1400202 and 15JC1400200), the National Science Foundation of China (NSFC) (31630044, 31601186, 31801228, and 81471948), External Cooperation Program of BIC, CSIRO-Chinese Academy of Science (153D31KYSB20150085 and 153D31KYSB20160247), and China Postdoctoral Science Foundation (2017M620174 and 2018T110412).

AUTHOR CONTRIBUTIONS

K.Z. and L.Z. designed and performed most of the experiments. X.M. and L.Z. analyzed the RNA-seq data. J.C. and Z.S. assisted with hepatocyte transplantation. C.W., Z. Zhang, L.S., Z. Zhu, L.Y., X. Chen, A.F., and L.P. assisted with cell culture. W.L. and D.G. provided the wnt3a-conditioned medium. Z.J. and P.L. performed the analysis of CYP2D6 activity *in vivo*. S.F., J.W., and X. Cheng assisted with the hepatic differentiation. L.Z., K.Z., and L.H. analyzed the data and wrote the manuscript. L.H. supervised and coordinated the project.

DECLARATION OF INTERESTS

The authors declare no competing interests.

Received: April 12, 2018
Revised: September 17, 2018
Accepted: October 12, 2018
Published: November 8, 2018

REFERENCES

Azuma, H., Paulk, N., Ranade, A., Dorrell, C., Al-Dhalimy, M., Ellis, E., Strom, S., Kay, M.A., Finegold, M., and Grompe, M. (2007). Robust expansion of human hepatocytes in Fah-/-/Rag2-/-/Il2rg-/- mice. Nat. Biotechnol. *25*, 903–910.

Azzolin, L., Panciera, T., Soligo, S., Enzo, E., Bicciato, S., Dupont, S., Bresolin, S., Frasson, C., Basso, G., Guzzardo, V., et al. (2014). YAP/TAZ incorporation in the β-catenin destruction complex orchestrates the Wnt response. Cell *158*, 157–170.

Bell, C.C., Hendriks, D.F., Moro, S.M., Ellis, E., Walsh, J., Renblom, A., Fredriksson Puigvert, L., Dankers, A.C., Jacobs, F., Snoeys, J., et al. (2016). Characterization of primary human hepatocyte spheroids as a model system for drug-induced liver injury, liver function and disease. Sci. Rep. *6*, 25187.

Bhatia, S.N., Underhill, G.H., Zaret, K.S., and Fox, I.J. (2014). Cell and tissue engineering for liver disease. Sci. Transl. Med. *6*, 245sr2.

Damalas, A., Kahan, S., Shtutman, M., Ben-Ze'ev, A., and Oren, M. (2001). Deregulated beta-catenin induces a p53- and ARF-dependent growth arrest and cooperates with Ras in transformation. EMBO J. *20*, 4912–4922.

Dhawan, A., Puppi, J., Hughes, R.D., and Mitry, R.R. (2010). Human hepatocyte transplantation: current experience and future challenges. Nat. Rev. Gastroenterol. Hepatol. *7*, 288–298.

Du, Y., Wang, J., Jia, J., Song, N., Xiang, C., Xu, J., Hou, Z., Su, X., Liu, B., Jiang, T., et al. (2014). Human hepatocytes with drug metabolic function induced from fibroblasts by lineage reprogramming. Cell Stem Cell *14*, 394–403.

Gao, Y., Zhang, X., Zhang, L., Cen, J., Ni, X., Liao, X., Yang, C., Li, Y., Chen, X., Zhang, Z., et al. (2017). Distinct gene expression and epigenetic signatures in hepatocyte-like cells produced by different strategies from the same donor. Stem Cell Reports *9*, 1813–1824.

Grompe, M., al-Dhalimy, M., Finegold, M., Ou, C.N., Burlingame, T., Kennaway, N.G., and Soriano, P. (1993). Loss of fumarylacetoacetate hydrolase is responsible for the neonatal hepatic dysfunction phenotype of lethal albino mice. Genes Dev. *7* (12A), 2298–2307.

Hasegawa, M., Kawai, K., Mitsui, T., Taniguchi, K., Monnai, M., Wakui, M., Ito, M., Suematsu, M., Peltz, G., Nakamura, M., and Suemizu, H. (2011). The reconstituted 'humanized liver' in TK-NOG mice is mature and functional. Biochem. Biophys. Res. Commun. *405*, 405–410.

Huang, P., Zhang, L., Gao, Y., He, Z., Yao, D., Wu, Z., Cen, J., Chen, X., Liu, C., Hu, Y., et al. (2014). Direct reprogramming of human fibroblasts to functional and expandable hepatocytes. Cell Stem Cell *14*, 370–384.

Huch, M., Gehart, H., van Boxtel, R., Hamer, K., Blokzijl, F., Verstegen, M.M.A., Ellis, E., van Wenum, M., Fuchs, S.A., de Ligt, J., et al. (2015). Long-term culture of genome-stable bipotent stem cells from adult human liver. Cell *160*, 299–312.

Janda, C.Y., Dang, L.T., You, C., Chang, J., de Lau, W., Zhong, Z.A., Yan, K.S., Marecic, O., Siepe, D., Li, X., et al. (2017). Surrogate Wnt agonists that phenocopy canonical Wnt and β-catenin signalling. Nature *545*, 234–237.

Ji, S., Zhang, L., and Hui, L. (2013). Cell fate conversion: direct induction of hepatocyte-like cells from fibroblasts. J. Cell. Biochem. *114*, 256–265.

Kang, L.I., Mars, W.M., and Michalopoulos, G.K. (2012). Signals and cells involved in regulating liver regeneration. Cells *1*, 1261–1292.

Katsuda, T., Kawamata, M., Hagiwara, K., Takahashi, R.U., Yamamoto, Y., Camargo, F.D., and Ochiya, T. (2017). Conversion of terminally committed hepatocytes to culturable bipotent progenitor cells with regenerative capacity. Cell Stem Cell *20*, 41–55.

Khetani, S.R., and Bhatia, S.N. (2008). Microscale culture of human liver cells for drug development. Nat. Biotechnol. *26*, 120–126.

Kidambi, S., Yarmush, R.S., Novik, E., Chao, P., Yarmush, M.L., and Nahmias, Y. (2009). Oxygen-mediated enhancement of primary hepatocyte metabolism, functional polarization, gene expression, and drug clearance. Proc. Natl. Acad. Sci. USA *106*, 15714–15719.

Kobayashi, N., Fujiwara, T., Westerman, K.A., Inoue, Y., Sakaguchi, M., Noguchi, H., Miyazaki, M., Cai, J., Tanaka, N., Fox, I.J., and Leboulch, P. (2000). Prevention of acute liver failure in rats with reversibly immortalized human hepatocytes. Science *287*, 1258–1262.

Kopp, J.L., Grompe, M., and Sander, M. (2016). Stem cells versus plasticity in liver and pancreas regeneration. Nat. Cell Biol. *18*, 238–245.

Leontieva, O.V., Natarajan, V., Demidenko, Z.N., Burdelya, L.G., Gudkov, A.V., and Blagosklonny, M.V. (2012). Hypoxia suppresses conversion from proliferative arrest to cellular senescence. Proc. Natl. Acad. Sci. USA *109*, 13314–13318.

Levy, G., Bomze, D., Heinz, S., Ramachandran, S.D., Noerenberg, A., Cohen, M., Shibolet, O., Sklan, E., Braspenning, J., and Nahmias, Y. (2015). Long-term culture and expansion of primary human hepatocytes. Nat. Biotechnol. *33*, 1264–1271.

Li, D., Li, W., and Hui, L. (2016). Hybrid hepatocyte: a newly identified player for regeneration in hepatic injuries. Hepatology *64*, 2244–2246.

Masubuchi, Y., Iwasa, T., Hosokawa, S., Suzuki, T., Horie, T., Imaoka, S., Funae, Y., and Narimatsu, S. (1997). Selective deficiency of debrisoquine 4-hydroxylase activity in mouse liver microsomes. J. Pharmacol. Exp. Ther. *282*, 1435–1441.

Michalopoulos, G.K. (2014). The liver is a peculiar organ when it comes to stem cells. Am. J. Pathol. *184*, 1263–1267.

Michalopoulos, G.K., and Khan, Z. (2015). Liver stem cells: experimental findings and implications for human liver disease. Gastroenterology *149*, 876–882.

Mitaka, T. (1998). The current status of primary hepatocyte culture. Int. J. Exp. Pathol. *79*, 393–409.

Miyajima, A., Tanaka, M., and Itoh, T. (2014). Stem/progenitor cells in liver development, homeostasis, regeneration, and reprogramming. Cell Stem Cell *14*, 561–574.

Parinello, S., Samper, E., Krtolica, A., Goldstein, J., Melov, S., and Campisi, J. (2003). Oxygen sensitivity severely limits the replicative lifespan of murine fibroblasts. Nat. Cell Biol. *5*, 741–747.

Rezvani, M., Grimm, A.A., and Willenbring, H. (2016). Assessing the therapeutic potential of lab-made hepatocytes. Hepatology *64*, 287–294.

Runge, D., Michalopoulos, G.K., Strom, S.C., and Runge, D.M. (2000). Recent advances in human hepatocyte culture systems. Biochem. Biophys. Res. Commun. *274*, 1–3.

Sampaziotis, F., Segeritz, C.P., and Vallier, L. (2015). Potential of human induced pluripotent stem cells in studies of liver disease. Hepatology *62*, 303–311.

Shan, J., Schwartz, R.E., Ross, N.T., Logan, D.J., Thomas, D., Duncan, S.A., North, T.E., Goessling, W., Carpenter, A.E., and Bhatia, S.N. (2013). Identification of small molecules for human hepatocyte expansion and iPS differentiation. Nat. Chem. Biol. *9*, 514–520.

Shih, H.P., Seymour, P.A., Patel, N.A., Xie, R., Wang, A., Liu, P.P., Yeo, G.W., Magnuson, M.A., and Sander, M. (2015). A gene regulatory network cooperatively controlled by Pdx1 and Sox9 governs lineage allocation of foregut progenitor cells. Cell Rep. *13*, 326–336.

Tanimizu, N., Nishikawa, Y., Ichinohe, N., Akiyama, H., and Mitaka, T. (2014). Sry HMG box protein 9-positive (Sox9+) epithelial cell adhesion molecule-negative (EpCAM-) biphenotypic cells derived from hepatocytes are involved in mouse liver regeneration. J. Biol. Chem. *289*, 7589–7598.

Tarlow, B.D., Pelz, C., Naugler, W.E., Wakefield, L., Wilson, E.M., Finegold, M.J., and Grompe, M. (2014). Bipotential adult liver progenitors are derived from chronically injured mature hepatocytes. Cell Stem Cell *15*, 605–618.

Wang, B., Zhao, L., Fish, M., Logan, C.Y., and Nusse, R. (2015). Self-renewing diploid Axin2(+) cells fuel homeostatic renewal of the liver. Nature *524*, 180–185.

Wu, H., Zhou, X., Fu, G.B., He, Z.Y., Wu, H.P., You, P., Ashton, C., Wang, X., Wang, H.Y., and Yan, H.X. (2017). Reversible transition between hepatocytes and liver progenitors for in vitro hepatocyte expansion. Cell Res. *27*, 709–712.

Yanger, K., Zong, Y., Maggs, L.R., Shapira, S.N., Maddipati, R., Aiello, N.M., Thung, S.N., Wells, R.G., Greenbaum, L.E., and Stanger, B.Z. (2013). Robust cellular reprogramming occurs spontaneously during liver regeneration. Genes Dev. *27*, 719–724.

Yimlamai, D., Christodoulou, C., Galli, G.G., Yanger, K., Pepe-Mooney, B., Gurung, B., Shrestha, K., Cahan, P., Stanger, B.Z., and Camargo, F.D. (2014). Hippo pathway activity influences liver cell fate. Cell *157*, 1324–1338.

Yoon, S.M., Gerasimidou, D., Kuwahara, R., Hytiroglou, P., Yoo, J.E., Park, Y.N., and Theise, N.D. (2011). Epithelial cell adhesion molecule (EpCAM) marks hepatocytes newly derived from stem/progenitor cells in humans. Hepatology *53*, 964–973.

STAR★METHODS

KEY RESOURCES TABLE

REAGENT or RESOURCE	SOURCE	IDENTIFIER
Antibodies		
Goat anti-human-Albumin	Bethyl Laboratories	Cat#A80-229A; RRID: AB_67018
Mouse anti-Hnf4α	Santa Cruz	Cat#SC-374229; RRID: AB_10989766
Rabbit anti-FAH	Gift from Dr. Xin Wang	Cat#N/A; RRID: N/A
Mouse anti-human CYP3A4	Santa Cruz	Cat#SC-53850; RRID: AB_782375
Mouse anti-Glutamine Synthase	BD bioscience	Cat#610517; RRID: AB_397879
Rabbit anti-SOX9	Millipore	Cat#Ab5535; RRID: AB_2239761
Mouse anti-CK19	Genetex	Cat#GTX84251; RRID: AB_10729890
Mouse anti-CK7	Abcam	Cat#Ab9021; RRID: AB_306947
Cy5-conjugated donkey anti-goat IgG	Jackson Lab	Cat#705-175-147; RRID: AB_2340415
FITC-conjugated donkey anti-rabbit IgG	Jackson Lab	Cat#711-095-152; RRID: AB_2315776
Cy3-conjugated donkey anti-rabbit IgG	Jackson Lab	Cat#711-165-152; RRID: AB_2307443
Cy3-conjugated donkey anti-mouse IgG	Jackson Lab	Cat#715-165-150; RRID: AB_2340813
FITC-conjugated donkey anti-mouse IgG	Jackson Lab	Cat#715-095-151; RRID: AB_2335588
Chemicals, Peptides, and Recombinant Proteins		
N-acetyl-cysteine	Sigma-Aldrich	Cat#A9165-100G
Nicotinamide	Solarbio	Cat#N8070
Recombinant humanFGF10	Peprotech	Cat#100-26
Recombinant human EGF	Peprotech	Cat#AF-100-15
Recombinant human HGF	Peprotech	Cat#100-39
Human [Leu15]-gastrin I	Sigma-Aldrich	Cat#G9145
A83-01	Tocris Bioscience	Cat#2939
Rho kinase inhibitor Y-27632	Selleck	Cat#s1049
Wnt3a protein	Stemimmune LLC	Cat#MST-WT3a-0010
Fetal bovine serum	Ausbian	Cat#VS500T
Penicillin-Streptomycin	Solarbio	Cat#P1400
Forskolin	Tocris Bioscience	Cat#2939
Dexamethasone	Sigma-Aldrich	Cat#D1756
Oncostatin M	Peprotech	Cat#300-10H
Critical Commercial Assays		
Human albumin ELISA Quantitation Set	Bethyl Laboratory	Cat#E80-129
Urea assay kit	Abnova	Cat#STA-392
Senescence Associated β-galactosidase Staining	Beyotime	Cat#C0602
Deposited Data		
PHHs and ProliHHs RNA-seq data	This paper	GEO: GSE112866
Experimental Models: Cell Lines		
Human:hepatocytes – See Table S1	Celsis *In Vitro* Technologies (Blatimore, MD)	Cat#F00995-P;M00995-P
Human:HepG2 cell line	American Type Culture Collection (ATCC)	Cat#ATCC HB-8065
Human:Snu398 cell line	Korean Cell Line Bank (KCLB)	Cat#KCLB No.00398.1
Mouse:L-Wnt3a cell	Gift from Dr. Hans Clevers	N/A
Experimental Models: Organisms/Strains		
Mouse: *Fah*$^{-/-}$*Rag2*$^{-/-}$*Il2rg*$^{-/-}$	Azuma et al., 2007	N/A
Mouse: NOD/SCID	Shanghai LinChang Biotech	N/A
Oligonucleotides		
Primers for q-PCR – See Table S2	This paper	N/A

(*Continued on next page*)

Continued

REAGENT or RESOURCE	SOURCE	IDENTIFIER
Software and Algorithms		
GraphPad Prism5	GraphPad Software	Version 5.0.1
ImageJ	NIH	https://imagej.nih.gov/ij/
FlowJo software	Tomy Digital Biology	FlowJo 7.6
Other		
hESC-derived liver progenitor cell RNA-seq data	Shih et al., 2015	GEO: GSE61946
hiHeps and hiPSC-Heps RNA-seq data	Gao et al., 2017	GEO: GSE103078

CONTACT FOR REAGENT AND RESOURCE SHARING

Further requests for reagents may be directed to, and will be fulfilled by, the Lead Contact, Lijian Hui (ljhui@sibcb.ac.cn).

EXPERIMENTAL MODEL AND SUBJECT DETAILS

Human hepatocyte culture

We used cryopreserved human hepatocytes from twelve individuals provided by Celsis *In Vitro* Technologies (Blatimore, MD). The information of these donors was listed in the Table S1. No sex bias differences were detected during cell culture. The media used for medium screening, hepatocyte proliferation and maturation are listed in Table S3. The cryopreserved primary human hepatocytes were resuscitated in DMEM supplemented with 10% fetal bovine serum (Sigma-Aldrich) and seeded in a collagen-I-coated dish at 2×10^4 cells/cm^2. Then cells were cultured in 37°C, Normoxia (5% CO_2 incubator) or Hypoxia (5% O_2, 5% CO_2 incubator). The medium was changed to HM 10 hours after seeding and every 2 days thereafter. On day 6 of the primary culture, cells were trypsinized and then seeded at 3×10^4 cells/cm^2 in collagen-I-coated dishes. Medium was changed every 2 days. For hepatic maturation, ProliHHs were seeded at 8×10^4 cells/well in a 96-well plate (Kuraray CO.Ltd.) in HIM for 10 days.

L-Wnt3a cell culture

The L-Wnt3a cell was a gift from Dr. Hans Clevers and cultured in DEMEM with 10% FBS and Zecocin (125ug/ml). When the cells were confluent, the medium was changed to advanced DMEM/F-12 with 10%FBS. After two-day incubation, the supernatant was harvested as Wnt3a-conditioned medium. The activity of 30% Wnt3a-conditioned medium and Wnt3a protein (50ng/ml) was determined by TOP/FOP assay. Adequate activity is a TOP/FOP value > 25.

Mice

The Fah$^{-/-}$Rag2$^{-/-}$Il2rg$^{-/-}$(FRG) mice were obtained from Dr. Xin Wang. FRG mice are on the hybrid strain of C57BL/6J and 129S6/SvEvTac and fed with drinking water containing 7.5 mg/L NTBC (Synthesized by Capot Chemical, China). A mix of 8 to 12 weeks old male and female mice were used for transplantation and no sex bias differences were detected.

NOD/SCID mice were purchased from Shanghai LinChang Biotech. NOD/SCID mice were on the NOD strain background. 6 to 8 weeks old male mice were used for transplantation.

None of the animals used in these studies had been subjected to prior procedures and were drug and test naive. All animals were housed in a temperature- and light-controlled (12-h light/dark cycle) specific pathogen-free (SPF) animal facility, in individually ventilated cages always with companion mice. All animal experiments were performed according to protocols approved by the institutional animal care and use committee at Shanghai Institute of Biochemistry and Cell Biology.

METHOD DETAILS

Time-lapse imaging at a low cell density

Primary human hepatocytes were seeded at 2×10^4 cells/cm^2 in 6-well collagen-coated plates (Corning) in HM. The medium was changed every 2 days. Time-lapse imaging was performed using an incuCyte FLR. Phase contrast imaging was performed from D1 to D3 at 30 min-intervals and a video was produced for each analyzed field.

PCR

For most experiments, total RNA was isolated from cells by Trizol (Invitrogen). RNA extracted from freshly thawed PHHs was used as controls. 1 μg RNA was reverse transcribed into cDNA with M-MLV Reverse Transcriptase (Promega) according to manufacturer's instructions. PCR was performed with HiFi Taq polymerase (TransGen). Quantitative real-time PCR was performed with SYBR Premix Ex Taq (TaKaRa) on ABI StepOnePlus real-time PCR system (Applied Biosystems). All q-PCR data were performed with at least 2 repeats. Primer sequences are provided in the Table S2.

Human Albumin ELISA

To determine the secretion of human Albumin, supernatants of cell culture were collected from 12-well plate after 24-hour culture. For transplantation experiments, animal serum was collected. Levels of human albumin were measured by the human albumin ELISA Quantitation Set (Bethyl Laboratory) according to the manufacturer's instructions. Serum was diluted in a range from 10- to 100000-fold to obtain values falling to the linear range of standard curve.

Urea synthesis assay

To determine the urea secretion, supernatants of cell culture were collected from 12-well plate after 24-hour culture. The concentration of secreted urea was measured by urea assay kit (Abnova) according to the manufacturer's instructions.

Histology, immunohistochemistry and immunofluorescence staining

Liver tissue samples were fixed overnight in 4% neutral buffered paraformaldehyde (Solarbio), embedded in paraffin, cut into 5 μm thick sections, and placed on adhesion microscope slides. Sections were subjected to hematoxylin-eosin (H&E), immunohistochemical (IHC) or immunofluorescence (IF) staining. IHC staining was performed using the Elite ABC kit (Vector Laboratories). For immunohistochemistry, deparaffinized and rehydrated slides were subjected to autoclave antigen retrieval in a 10 mmol/L citric acid buffer (pH 6.0) and allowed to cool to room temperature. Slides were blocked with 3% H_2O_2 for 30 minutes, washed in phosphate-buffered saline, then blocked with 5% normal goat serum in PBS. Slides were incubated with diluted primary antibodies overnight at 4°C. The following primary antibody was used: rabbit anti-FAH (gift from Dr. Xin Wang, 1:3000).

For immunofluorescent staining, the cells were fixed with 4% paraformaldehyde for 15 min at room temperature, and then incubated with PBS containing 0.2% Triton X-100 (Sigma) for 15 min. Cells were then washed three times with PBS. After being blocked by 3% BSA in PBS for 60 min at room temperature, cells were incubated with primary antibodies at 4°C overnight, washed three times with PBS, and then incubated with appropriate fluorescence-conjugated secondary antibody for 60 min at room temperature in dark. Nuclei were stained with DAPI (Sigma). Primary and secondary antibodies were diluted in PBS containing 3% BSA.

Antibodies used for immunofluorescent staining are as follows: goat anti-human-Albumin (Bethyl Laboratories, 1:200), mouse anti-Hnf4α (Santa Cruz, 1:200), rabbit anti-FAH (gift from Dr.Wang xin's Lab, 1:3000), mouse anti-human CYP3A4 (Santa Cruz, 1:200), mouse anti-GS (BD, 1:100), rabbit anti-SOX9 (Millipore, 1:1000), mouse anti-CK19 (Genetex, 1:200), mouse anti-CK7 (Abcam, 1:200), Cy5-conjugated donkey anti-goat IgG (Jackson Lab, 1:500), FITC-conjugated donkey anti-rabbit IgG (Jackson Lab, 1:500), Cy3-conjugated donkey anti-rabbit IgG (Jackson Lab, 1:500), Cy3-conjugated donkey anti-mouse IgG (Jackson Lab, 1:1000), FITC-conjugated donkey anti-mouse IgG (Jackson Lab, 1:1000).

Assays for PAS and Oil Red O staining

Cells were stained by Periodic-Acid-Schiff (PAS, Sigma) following manufacturer's instructions. For Oil red staining, confluent cells were cultured in HM. After 4 days, cells were washed twice with PBS (Hyclone), fixed in 4% formalin for 30 min, washed by PBS, followed by Oil Red (Sigma-Aldrich) staining for 10 min, and then washed twice by 70% ethanol.

Senescence-Associated β-Galactosidase Analysis

For senescence-associated β-galactosidase (SA-β-gal) staining, the cells were fixed with 4% paraformaldehyde for 5 min at room temperature. Cells were stained by Senescence Associated β-galactosidase Staining (Beyotime) following manufacturer's instructions.

CYP metabolism assay

For measurement of CYP2B6 metabolism activity, ProliHHs were cultured in a 96-well plate (Kuraray CO.Ltd.) in HIM for 10 days. Freshly thawed primary human hepatocytes were directly used as a positive control. Cells were incubated with substrate in 200 μL incubation medium for 3 hours at 37°C. To stop the reaction, 800 ul cold methanol was added and centrifuged. For measurement of CYP2D6 metabolism activity,the serum (50ul) was collected from control FRG mice and ProliHH-FRG mice at 0, 0.5, 1, 2 h after administration of DEB (2mg/kg, Sigma). The supernatants were collected for measurement of metabolized compounds by LC-MS/MS (Agilent 1200 HPLC and ABI 4000 mass-spectrometer). Substrates and metabolized products used for standard curves were commercially purchased.

Transplantation of cells into $Fah^{-/-}Rag2^{-/-}Il2rg^{-/-}$mice

Six days before cells transplantation, concentration of NTBC in drinking water for FRG mice was first reduced to 3.75 mg/L for 3 days and was then totally withdrawn for another 3 days. $5x10^5$ ProliHHs at early passages (before P4) and late passages (after P6) and PHH in 100 μL PBS were intrasplenically transplanted into FRG mice. After transplantation, NTBC was transiently put on for three days when mice lost 20% of their body weights. Mice were sacrificed 4 or 5 months later.

Tumor formation assay

For the tumor generation assay, human hepatoma cell line SNU398 was used as positive control. ProliHHs were cultured as described above. Cells were detached by trypsin and suspended in PBS. 2×10^6 ProliHHs and SNU398 cells were subcutaneously injected to NOD/SCID mice. Tumor numbers were counted 8 weeks after injection.

QUANTIFICATION AND STATISTICAL ANALYSIS

RNA-sequencing data process

Total RNA was extracted using Trizol according to the manufacturer's instructions. Sequencing library was prepared from one microgram of total RNA using Illumina TruSeq RNA Sample Prep Kit. Double-end 100 bp read length sequencing was performed on Illumina Hiseq 2000 sequencer. The reads were mapped to the human reference genome (hg19) using Tophat. FPKM (fragments per kilobaseof exon per million fragments mapped) values for UCSC genes were calculated by Cufflinks using default parameters. The FPKM were added with 1 and log2 transformed for downstream analysis. For gene expression analysis, a one-way ANOVA was performed to identify differentially expressed genes (DEGs). P values and fold-change numbers were calculated for each analysis. Unsupervised clustering was performed with sorted or whole genes using Cluster 3.0. Heatmap generation were performed with sorted or whole genes using the R package (pheatmap, function: pheatmap()). Principal component analysis was performed with whole genes using the R package (function: prcomp()).

Pathway enrichment analysis

Gene set enrichment analysis (GSEA) was used for pathway enrichment of DEGs. For the list of DEGs, online MSigDB tool was used (http://software.broadinstitute.org/gsea/msigdb/index.jsp). GSEA v2 desktop software was also used to identify the significantly enriched pathways from the RNaseq results.

Statistical Analyses

The number of biological and technical replicates and animals are indicated in figure legends and text. All data are presented as the mean ± SD. For most statistic evaluation, an unpaired Student's t test was applied for calculating statistical probability in this study. P values were calculated by two-tailed test. Only for survival analysis in Figure 5A, the Mantel-Cox log-rank test was applied. Statistic calculation was performed using GraphPad Prism5 (GraphPad). The liver repopulation efficiency of ProliHH and PHH was determined by taking representative images from different mice and directly counting Fah^{+} area ratio by ImageJ. Three to five liver areas from each mouse were analyzed.

DATA AND SOFTWARE AVAILABILITY

Data Resources

The accession number for the RNA-seq data reported in this paper is GEO: GSE112866.